

Local modulation of plus-end transport targets herpesvirus entry and egress in sensory axons

G. A. Smith*, L. Pomeranz†, S. P. Gross*§, and L. W. Enquist*^{§¶}

*Department of Microbiology-Immunology, Ward Building, Room 10-105, Northwestern University Feinberg School of Medicine, Chicago, IL 60611;

†Department of Developmental and Cell Biology, 2222 Natural Sciences I, University of California, Irvine, CA 92697; and §Department of Molecular Biology, Schultz Laboratory, Room 301, Princeton University, Princeton, NJ 08544-1014

Edited by David W. Tank, Princeton University, Princeton, NJ, and approved September 21, 2004 (received for review June 30, 2004)

The core structures of many viruses move within cells by association with host cytoskeletal motor proteins; however, the mechanisms by which intracellular viral particles are transported toward sites of replication or the cell periphery at distinct stages of infection remain to be understood. The regulation of herpesvirus directional transport in sensory neurons was examined by tracking individual viral capsids within axons at multiple frames per s. After entry into axons, capsids underwent bidirectional and saltatory movement to the cell body independently of endosomes. A comparison of entry transport to a previous analysis of capsid axonal transport during egress revealed that capsid targeting in and out of cells occurs by modulation of plus-end, but not minus-end, motion. Entry transport was unperturbed by the presence of egressing virus from a prior infection, indicating that transport direction is not modulated globally by viral gene expression, but rather directly by a component of the viral particle.

virus | neuron

The α -herpesviruses are parasites that reside within the vertebrate nervous system, but are typically restricted to the peripheral nervous system (PNS) of the natural host. Initial infection requires retrograde axonal transport of the herpesvirus capsid to the nuclei of neurons in peripheral ganglia, where latency is established. Reactivation from latency can occur throughout the life of the host, resulting in recurrent disease (e.g., herpes labialis produced by herpes simplex virus type 1 and shingles produced by varicella-zoster virus). Reactivated infection requires anterograde transport from ganglia back to exposed body surfaces, where infection can transmit to new hosts. That the mechanism of viral transport and its directional regulation remain to be discovered has important functional consequences: it allows rapid infection and spread without exposure to circulating immune defenses and plays an important role in determining the outcome of infection. Transsynaptic transport of infection from the PNS into the CNS is a rare but devastating progression of disease that typically results in fatal encephalitis (1–3).

The herpesvirus virion consists of a double-stranded DNA genome encased in an icosahedral capsid shell. The capsid is surrounded by an additional layer of proteins collectively called the “tegument,” which is in turn enveloped by a lipid bilayer containing viral membrane proteins. The viral genome is transported within capsids, either being released into the nucleus through nuclear pores during initial infection, or assembled with tegument and envelope into mature virions during final egress from a cell (reviewed in ref. 4).

By tracking individual pseudorabies virus (PRV; an α -herpesvirus of broad host range) capsids tagged with the GFP, we previously analyzed the dynamics of newly replicated capsids during egress in axons of infected sensory neurons (5). The GFP signal enabled tracking of individual \approx 125-nm capsids in living cells with a temporal resolution of 1–10 frames per s (fps). Although capsid transport was targeted to the terminal ends of axons as expected, individual capsids moved bidirectionally,

sometimes moving processively in the retrograde direction for prolonged periods. These findings stand in contrast to those reported for vaccinia virus where egress occurs by anterograde transport along microtubules without any retrograde motion (6, 7). Therefore, the significance of bidirectional transport during herpesvirus egress was not immediately clear.

Here, we describe the dynamics of herpesvirus capsids as they move from axon terminals to neuronal cell bodies during initial infection. As during egress, capsid transport is bidirectional; however, retrograde motion is now dominant. The dynamics of retrograde motion were statistically indistinguishable from the minor retrograde component previously observed during egress. To address whether this control was achieved by alteration of the global intracellular environment resulting from viral gene expression, we looked at the outcome of a secondary viral infection in previously infected cells. We found that newly infecting viral particles moved in a net retrograde direction toward the nucleus, even if the cell had a previous productive infection. Thus, entering virions seem able to locally control their direction of transport and can modulate the host transport machinery to achieve appropriate targeting. We conclude that capsid targeting to either the cell body or axon terminal is achieved by local regulation of the amount of plus-end-directed microtubule transport.

Materials and Methods

Virus and Cells. The recombinant isolate of PRV, PRV-GS443, expresses GFP fused to the VP26 capsid protein and has been described (5). PRV-GS847 is identical to PRV-GS443 but carries the monomeric red fluorescent protein (mRFP1) ORF in place of the GFP ORF, and is therefore a red-fluorescent analog of the GFP-capsid virus (8). PRV-GS847 was made by recombining the mRFP1 fusion into the pBecker3 infectious clone by RecA-dependent homologous recombination in *Escherichia coli* by using previously described methods (9). The GFP- and mRFP1-fluorescent capsid viruses were propagated, and titers were determined, on pig kidney epithelial cells (PK15). Titers were equivalent to wild-type virus ($\geq 1 \times 10^8$ plaque-forming units/ml). To make a virus deleted for the gD glycoprotein gene (Us6), the infectious clone encoding the GFP-VP26 capsid fusion (pGS443) was recombined with an amplified PCR product of a kanamycin selectable marker, resulting in insertion of the marker in Us6. The primers used for amplification of the kanamycin marker were as follows: 5'-GGGGCCCCAGGTT-CCCATACACTCACCTGCCAGCGCCATGTAAGAAGT-TCCTATACTTTCTAGAGAATAGGAACTTCCCAGT-CACGACGTTGTAAAACG and 5'-GGAAGAAGATGTAGACGCACACGCCACCAGGAGCG CGCCGAAGT-

This paper was submitted directly (Track II) to the PNAS office.

Abbreviations: PRV, pseudorabies virus; DRG, dorsal root ganglion; mRFP1, monomeric red fluorescent protein; TMR, tetramethylrhodamine; fps, frames per second.

§S.P.G. and L.W.E. contributed equally to this work.

¶To whom correspondence should be addressed. E-mail: lenquist@molbio.princeton.edu.

© 2004 by The National Academy of Sciences of the USA

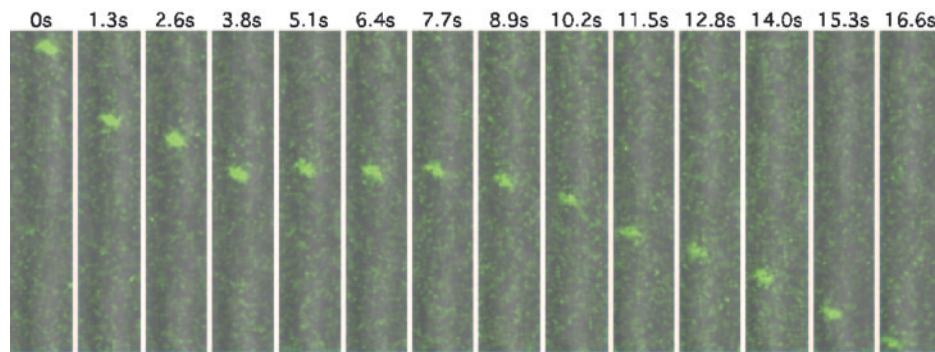


Fig. 1. Retrograde transport of GFP-capsids after entry. Shown is fluorescent time-lapse recording of an axon of a DRG sensory neuron. Images were captured by laser-scanning confocal microscopy of the field every 0.638 s after viral inoculation onto the cells (every other frame is shown). Differential interference contrast images were simultaneously captured by a back-side detector and were overlaid with the fluorescence images. A single capsid is seen moving from the top of the field to the bottom. The pause in motion is typical of the overall saltatory motion. The axon of the infected neuron was oriented with the cell body below the field of view, consistent with retrograde motion. (Area of field shown = $5.6 \times 28.0 \mu\text{m}$.) For a time-lapse recording of entry dynamics, see Movie 1, which is published as supporting information on the PNAS web site.

TCCTATTCTCTAGAAAGTATAGGAACTTCGAAAC-AGCTATGACCATGATTACG. The 5' end of each primer encodes 40 bp of homology flanking the region of Us6 targeted for deletion, and a 34-bp F1p recognition target (FRT) site is encoded by each primer (underlined sequence). The linear PCR product was recombined into pGS443 by RecA-independent homologous recombination in *E. coli* strain EL250, and the kanamycin marker was subsequently removed by F1p-mediated recombination of the two FRT sites (10). The resulting infectious clone (pGS791) encodes a stop codon (bolded in the first primer sequence) and a single 34-bp FRT site immediately after the ATG start codon, and deletes codons 2–361 of Us6 (400 codons total). The viral gD glycoprotein is responsible for blocking additional viral entry into an infected cell once viral gene expression is underway (11, 12). Because gD is also essential for production of infectious particles, pGS791 was transfected and propagated on G5 swine kidney cells, which constitutively express the PRV gD glycoprotein (in the absence of gD, PRV can egress from cells but the released viral particles are not infectious) (13).

Neuronal Culture. To allow for a direct comparison of newly acquired entry data with that previously collected during viral egress in axons, sensory neurons were isolated and maintained as described (5). Briefly, sensory neurons were cultured from dorsal root ganglia (DRG) of E8–E10 chick embryos, and were seeded on polyornithine-treated 22-mm-square glass coverslips at ≈ 100 neurons per coverslip. To allow for axon outgrowth, sensory neurons were cultured for 3–5 days before infection with PRV-GS443.

Infections and Time-Lapse Fluorescent Microscopy. Viral stocks harvested from porcine kidney 15 (PK15) cells were frozen, thawed, and sonicated (model VCX500; Sonics & Materials, Danbury, CT) before infection of sensory neurons. The viral stock was diluted 1:10 in HEPES-buffered media (pH 7.4), and $\approx 70 \mu\text{l}$ was used to fill a chamber made of a coverslip sealed above a glass slide by using a 1:1:1 mixture of Vaseline, beeswax, and lanolin. All samples were maintained at 37°C during imaging. With the exception of experiments using PRV-GS847 (see below), samples were imaged with a Zeiss 510 laser-scanning confocal microscope by using a 63×1.4 N.A. oil objective and a 488-nm argon laser line. This protocol is based on our previous study of capsid egress in axons, except that virus was added to neurons immediately before imaging (5). Steady-state fluorescent labeling of endosomes was achieved by incubating cells for 8–16 h in

media supplemented with 0.2 mg/ml 10,000 molecular weight dextran coupled to tetramethylrhodamine (TMR-dextran; Molecular Probes) (14). Cells were washed three times in media lacking TMR-dextran before infection. Simultaneous imaging of TMR-dextran and GFP-capsids was achieved with a 488/543-nm dual band dichroic mirror, and coexcitation with 543-nm HeNe and 488-nm argon laser lines. A 570-nm beam splitter was used with a 560-nm long pass (LP) filter to collect TMR emissions, and a downstream 490-nm beam splitter was used with a 505- to 530-nm band pass (BP) filter to collect GFP emission, thus allowing simultaneous imaging of both fluorophores on parallel photomultiplier tubes. Imaging of PRV-GS847 (see Fig. 4) was performed with a Nikon TE2000 inverted wide-field fluorescent microscope equipped with a 60×1.4 N.A. oil objective, Texas red filter set, and Roper Scientific (Tucson, AZ) Cascade charge-coupled device camera.

Image Analysis. GFP-capsids were tracked in axons by using the ISEE software package, as described (5). Motion was then parsed into periods of uninterrupted motion in a given direction (“runs”). Statistics were then compiled, keeping plus-end-directed runs and minus-end-directed runs separate. Storage of the GFP-containing viral stocks at -80°C and subjecting stocks to freeze/thaw and sonication before infection resulted in capsids with a broad distribution of reduced emissions. In general, fluorescent emissions were somewhat less variable when viral stocks were stored at -80°C for <1 week, and the emissions from individual GFP-particles were similar to those previously described (data not shown) (5).

Results

Imaging Viral Capsids During Entry. Previously, we used time-lapse fluorescent microscopy to image and track individual GFP-tagged capsids during egress transport from neuronal cell bodies to the distal ends of axons (which typically displayed growth cone morphology) of dissociated sensory neurons (5). In the work presented here, we use identical imaging techniques to track GFP-capsids immediately preceding entry from axon terminals to neuronal cell bodies (Fig. 1). Although similar in approach to the previous egress study, examination of entry was complicated by a reduced number of transport events per infection (owing to the small number of virions that enter cells after infection) and decreased GFP emissions from individual particles. The latter was likely a result of storage of the fluorescent viral stocks at -80° before infection. Capsid motion was tracked in dissociated sensory neurons from dorsal root ganglia of embryonic day 8

(E8)–E10 chick embryos. To confirm transport direction, only axons that could clearly be ascribed to a specific neuron or growth cone were analyzed; axons crossing or bundled with other axons were avoided. Capsids moved predominantly in the retrograde direction (toward the cell body). Entry transport was processive (occasionally capsids moved through the field of view, typically 30–40 μm , without pausing) and saltatory. Capsids also moved in the anterograde direction, although this motion was transient and followed by immediate reversal to retrograde motion. Nevertheless entry transport, like egress transport, was bidirectional (5).

Analysis of Motion During Viral Entry. Individual capsids were tracked through successive frames of time-lapse fluorescent recordings until they migrated out of the image field. Our temporal resolution ranged from 1–10 fps. Recordings were begun within 5 min of virus inoculation onto the cells (the majority of capsid entry transport in axons was observed within the first 30 min of infection). Occasionally, we observed a fluorescent capsid, diffusing in the tissue culture media, to make contact with a growth cone, and subsequently to initiate fast retrograde transport toward the cell body (in one instance, the capsid of a newly bound virion initiated retrograde axonal transport ≈ 1.5 min after the virion contacted the growth cone; see Movie 2, which is published as supporting information on the PNAS web site). In contrast, we never saw particles initiating infection at axon shafts.

Capsid dynamics were quantitated by analyzing periods of uninterrupted capsid travel in one direction (defined as a capsid run). A run ended when capsid motion paused, reversed direction, or was lost from the field of view. Because of the latter, a fraction of runs were truncated as a consequence of the small imaging area required to achieve optimal spatial resolution while maintaining temporal imaging faster than 1 fps. We analyzed 259 runs in the retrograde direction, the dominant component of entry transport. Retrograde runs had an average velocity of $1.17 \pm 0.03 \mu\text{m/s}$ (SEM) and were well modeled by a Gaussian distribution, indicating that a single class of minus-end-directed motor is likely responsible for capsid transport toward the cell body (Fig. 2). Top speeds for retrograde runs were in excess of 3 $\mu\text{m/s}$. These velocities were calculated as the average speed over the entire length of the run; instantaneous velocities had a wider distribution (not shown). The average length of retrograde runs was $7.38 \pm 0.47 \mu\text{m}$ (SEM), and the distribution of run lengths was fit by a decaying exponential as expected for processive motion. Runs that did not leave the image field typically ended by a reversal in direction; of the 259 retrograde runs analyzed, 68 reversals were observed. We did not observe prolonged anterograde capsid transport; rather, reversal events were short-lived (lasting ≈ 0.9 s on average) and always ended in an immediate reversal to retrograde motion. Because the average time span of the anterograde runs was in the range of our temporal resolution, quantitation of anterograde dynamics was inherently less accurate. With this caveat, we measured an average velocity of $0.55 \pm 0.05 \mu\text{m/s}$ (SEM) and run length of $0.40 \pm 0.03 \mu\text{m}$ (SEM). In addition to reversals, we observed 27 runs end in loss of motion, which lasted on average for 1.41 ± 0.38 s (SEM) and had an upper observed limit of 10 s. Unlike motion during egress, these pauses in motion were transient, and permanent stalls were rare (9). We cannot rule out the possibility that many observed pauses in retrograde motion were short-lived reversal events below our temporal or spatial resolution.

Capsids and Endosomes Traffic Independently in Axons. Although transmission electron microscopy studies of herpesviruses infections in sensory neurons support a model of viral entry by fusion at the host cell plasma membrane, endocytosis of virions can result in productive infections in some cell types (15, 16). To

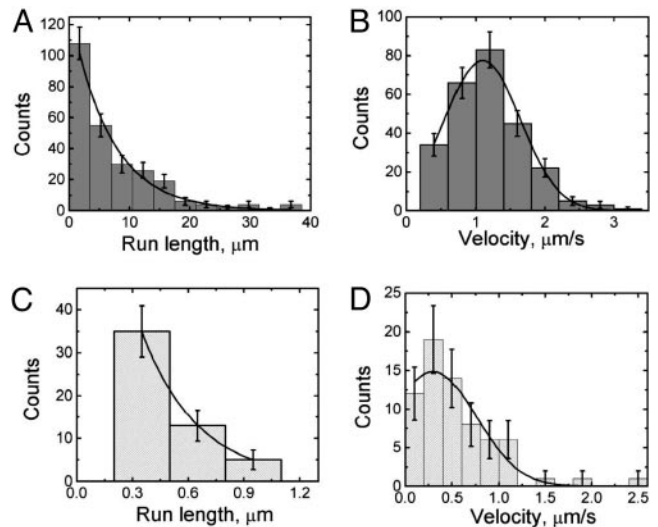


Fig. 2. Parameters of capsid motion during entry. Histograms of the processivities and velocities of retrograde motion during entry are shown in A and B. A similar analysis of the minor anterograde component is shown in C and D. The distribution of minus-end run lengths (A) is reasonably modeled by a single decaying exponential functional form with a decay length of $6.7 \pm 0.6 \mu\text{m}$ ($\chi^2 = 1.09$; $df = 5$). Note that there could be a short (undetected) population of runs, as our spatial and temporal resolution does not permit us to accurately resolve short runs (less than ≈ 400 nm in length). The distribution of minus-end velocities, calculated by dividing the spatial run length by its temporal duration (B), is well modeled by a Gaussian functional form centered at $1.10 \pm 0.03 \mu\text{m/s}$ and a width of $1.1 \pm 0.05 \mu\text{m/s}$ ($\chi^2 = 0.52$; $df = 3$). The distribution of plus-end runs (C) seems reasonably described by a single decaying exponential functional form with a decay length of $\approx 0.3 \mu\text{m}$, but this result should be viewed as an estimate only, because many of the short runs are likely below the limit of our current resolution (a meaningful χ^2 value could not be determined due to these limitations). Similarly, our data suggest that the distribution of plus-end velocities (D) is reasonably modeled by a Gaussian functional form centered at $0.30 \pm 0.16 \mu\text{m/s}$ and a width of $0.92 \pm 0.28 \mu\text{m/s}$. Error bars are expected uncertainty, assuming Gaussian statistics for all graphs.

determine whether axonal transport of capsids was associated with endosome transport, sensory neurons and nonneuronal cells present in the disassociated neural culture were together infected with the GFP-capsid virus after labeling of the endocytic pathway with a TMR-dextran fluid-phase marker. Although GFP-capsid emissions were frequently observed in endosomes of a sub population of nonneuronal cells [presumably Schwann cells (17)], GFP-capsids never colocalized with the TMR-dextran label in axons (Fig. 3).

Comparison of Entry and Egress Capsid Transport. By analyzing entry and egress capsid transport dynamics by identical methods, a comparison of capsid motion is practical (9). Although the anterograde components of motion during entry and egress transport were distinct, retrograde transport was statistically indistinguishable both in terms of velocity and run length (Table 1).

Although the mechanism by which alteration of anterograde motion is achieved is not immediately clear, modulation of capsid anterograde motion may result from global changes in the cellular environment resulting from viral gene expression (i.e., egress targeting of capsids could be effected by a general reconfiguration of the axonal transport machinery). To examine this possibility, we infected neurons with a GFP-capsid virus and then superinfected these same neurons 13 h later with a mRFP1-capsid virus and examined the entry dynamics of the red-fluorescent capsids in the context of an infected cell. Because herpesvirus infection of cultured DRG sensory neurons results

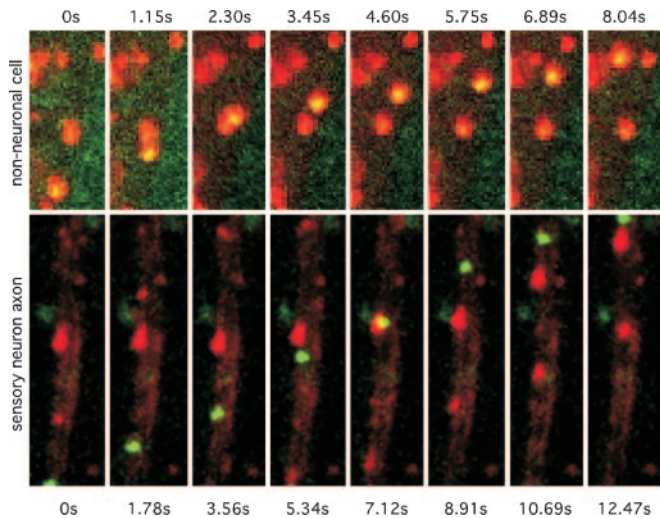


Fig. 3. Herpesvirus transport in axons is independent of endosomal trafficking. Cultures of dissociated chick DRG were labeled to steady state with TMR-dextran as an endocytic tracer. GFP-capsid emissions were frequently associated with endosomes in nonneuronal cells present in the DRG cultures but were never localized to endosomes in axons. (Upper) An example of an endosomal capsid transporting in a nonneuronal cell is shown (area of field shown = $4 \times 9 \mu\text{m}$; capsid/endosome velocity $\approx 0.9 \mu\text{m/s}$). (Lower) Independent retrograde transport of a capsid and endosomes in a sensory neuron axon (area of field shown = $10 \times 36 \mu\text{m}$; capsid velocity $\approx 2.8 \mu\text{m/s}$). For complete time-lapse recordings, see Movies 3 and 4, which are published as supporting information on the PNAS web site.

in a block to additional viral entry beginning 2–4 h postinfection (18), we used a gD-null derivative of the GFP-capsid virus for the primary infection [superinfection is not blocked by viruses lacking the gD gene (11, 12)] to make this experiment feasible. Cells undergoing productive infection with the GFP-capsid/gD-null virus were observed to support typical net retrograde transport of newly infected mRFP1-capsid virus (Fig. 4).

Discussion

The genomes of neurotropic herpesviruses must travel long distances in sensory axons of the peripheral nervous system both to establish life-long infection and to reinfect peripheral tissue upon reactivation to spread between hosts. By an unknown mechanism, this process is effected by targeting axonal transport of viral capsids in either the retrograde (toward sensory ganglia) or anterograde (toward the periphery) direction at distinct phases of the infectious cycle. Inadvertent anterograde targeting of the virus may result in devastating forms of encephalitis (19).

Because endogenous vesicle-bound cargoes move in both the anterograde and retrograde directions in axons (14, 20–24), targeted herpesvirus capsid transport could be explained if capsids were present in host vesicles. For example, some neurotropic viral pathogens, such as poliovirus, enter axons by endocytosis and subsequently traverse the axon in the endo-

some (25). However, by transmission electron microscopy (TEM), herpesvirus capsids are typically observed directly in the cytosol subsequent to entry into axons (15, 26, 27). Similarly, we see membrane-free capsids in axons in our culture model by TEM (data not shown). Consistent with static TEM images, we find that, by imaging both capsids and the endosomal pathway simultaneously in living cells, retrograde transport of capsids in axons is mediated independently of endosome transport. During egress, progeny capsids have also been reported to transport independently of membranes and viral membrane proteins (28–31). Together, these findings indicate that capsid targeting is modulated by virus-encoded factors rather than by default endocytic and biosynthetic pathways of the neuron. For most virus stocks, a fraction of virions fail to initiate infection for a variety of possible reasons. Therefore, it is important to note that all of the particles tracked in this study were competent to enter axons and were not retained in endosomes. We expect that, despite our inability to determine their subsequent fate, the transport of particles must be an important step in the productive infection of neurons.

By comparative analysis of our studies on the dynamics of entry and egress in sensory axons, we make four principle conclusions. First, permanent loss of capsid motion (stalling) during translocation in axons is observed only during egress. The reason is unclear but may result from egress of viral particles from the cell interior to the outer surface of the axon, either at the axon terminal, or less frequently mid-axon.

Second, axonal transport of capsids is consistently bidirectional. Our examinations of entry and egress both show that reversals of direction are often observed to be instantaneous even at a temporal resolution of 30 fps (data not shown). This observation indicates that capsids associate with a bidirectional transport apparatus. Although many endogenous cargoes undergo coordinated bidirectional motion in association with microtubules, the molecular nature of the putative bidirectional motor complex has yet to be discerned [recently, however, biochemical links between kinesins and dynein/dynactin have been identified (32, 33)]. Although several herpesvirus proteins can bind host motor proteins *in vitro* and in two-hybrid studies, no virus/host interactions have been identified that are required for capsid transport (34–37).

Third, the kinetics of retrograde motion during entry and egress were statistically identical. The simplest explanation is that a minus-end-directed motor, presumably dynein (38, 39), is active at capsid surfaces during both stages of the infectious cycle. More importantly, the similarity of minus-end transport in both cases suggests that overall capsid transport in both entry and egress is due to the same transport machinery, functioning in much the same way in both instances. In principle, capsid motion could involve completely different processes during entry and egress. For instance, as the outer makeup of the capsid could change during entry versus egress (possibly due to the presence or absence of particular viral tegument proteins), one could imagine that entirely different transport machinery could be recruited to move the capsid in these two cases. The fact that the minus-end motion is the same in both entry and egress suggests that this is not the case.

Fourth, the anterograde component of transport is modulated (Fig. 5). We note that, although the processivity of plus-end motion is clearly reduced during entry transport, the reduction in velocity may manifest from our inability to fully resolve the short anterograde runs characteristic of entry dynamics in the present study. Preliminary observations attained at 30 fps indicate that instantaneous plus-end velocities during entry and egress may be equivalent (data not shown). This finding is consistent with work characterizing motion in other bidirectional transport systems including mitochondria,

Table 1. Summary of entry and egress data

| | Velocity | Run length | <i>n</i> |
|-------------|-------------------------------|-----------------------------|----------|
| Entry | | | |
| Anterograde | $0.55 \pm 0.05 \mu\text{m/s}$ | $0.4 \pm 0.03 \mu\text{m}$ | 68 |
| Retrograde | $1.17 \pm 0.03 \mu\text{m/s}$ | $7.38 \pm 0.47 \mu\text{m}$ | 259 |
| Egress | | | |
| Anterograde | $1.97 \pm 0.06 \mu\text{m/s}$ | $13.1 \pm 0.6 \mu\text{m}$ | 198 |
| Retrograde | $1.28 \pm 0.12 \mu\text{m/s}$ | $6.8 \pm 1.2 \mu\text{m}$ | 33 |

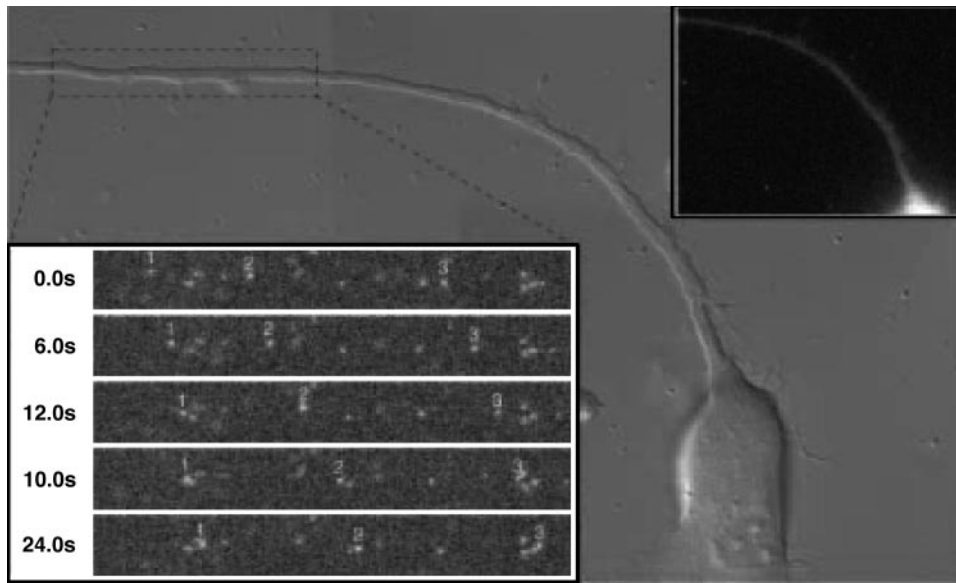


Fig. 4. Entry transport is not blocked in a late-stage infected neuron. In superinfected neurons, newly entering viruses display net retrograde motion typical of normal infections. Neurons were first infected with PRV-GS791, which expresses a GFP-capsid but is deleted for the gD glycoprotein. The deletion inhibits the herpesvirus block to superinfection, allowing for subsequent infection with a second virus (PRV-GS847, which expresses a mRFP1-capsid). Superinfection was begun at 13.5 h post initial infection, allowing for PRV-GS791 progeny virus to egress before addition of PRV-GS847. The imaged neuron is shown in the background in three overlapping differential interference contrast images. GFP imaging showed the neuron to be in the late stages of infection from the first virus (PRV-GS791), as indicated by the oversaturated fluorescence emitting from the soma (due to capsid assembly and maturation) and two capsids in the axon (*Inset*, top right). Retrograde capsid transport of PRV-GS847 was monitored by red emission, and three capsids undergoing entry transport toward the soma are shown (*Inset*, bottom left; area of field shown = $68 \times 9 \mu\text{m}$). Additional dim punctae are extracellular virions that bound to the axon shaft but did not enter (and were partly bleached during imaging).

Xenopus pigment granule melanophores, and *Drosophila* lipid droplets (40–43). In these systems, there is coordination between the opposite polarity motors, and the direction of net

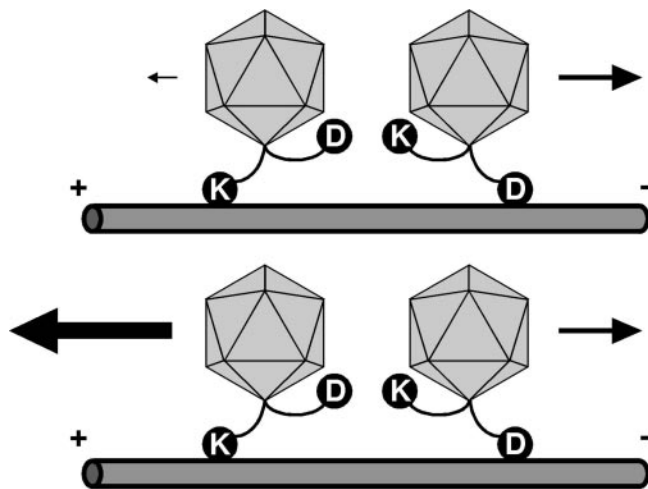


Fig. 5. Coordination of a bidirectional motor complex directs capsid transport. Shown is a model contrasting transport dynamics of herpesvirus capsids during entry and egress. Dynein (D) and a kinesin family (KIF; K) motor are illustrated bound to individual capsids simultaneously as part of a coordinated bidirectional motor complex. A direct interaction of capsids with motor complexes is shown for illustrative purposes only. The interaction of motors with cargo or each other could be direct or indirect by means of additional proteins. Net retrograde motion required for entry results when the contribution of the KIF motor in the complex is reduced (*Upper*). Alternatively, increasing the KIF contribution results in net anterograde motion required for egress (*Lower*). The contribution of the dynein motor does not change during entry and egress in this model.

transport is determined by altering the amount of plus-end motion while leaving the minus-end motion constant. Because the same seems true here, virus particles may be recruiting a complete bidirectional transport apparatus similar to one used in those systems. Significantly, in two of the previously described systems, there is a key difference: in the melanophores, transport is controlled by a global signal (cAMP/PKA) whereas, for the lipid droplets, a globally acting directionality factor (Halo) determines the amount of plus-end motion of all lipid droplets in the embryo (44, 45). In contrast, global changes in the infected cell are not responsible for differential capsid motion during egress versus entry: the ability of capsids newly deposited into the axon during superinfection to undergo typical retrograde motion indicates that local changes in capsid structure modulate appropriate targeting. This result may be explained if the virion substructure binds a kinase or phosphatase that modifies associated host motor complexes. Alternatively, a viral tegument protein acts locally at the capsid surface to function analogously to the Halo protein (which presumably localizes to the lipid droplets to alter plus-end motion) (45). These possibilities are not mutually exclusive, as two viral-encoded tegument proteins are serine/threonine kinases (46–49). Regulation of a kinesin motor may allow for dynein activity to become processive (50). Little is currently known regarding the composition of the capsid/tegument structure during intracellular transport, particularly during entry transport, although there is some evidence for transport of tegument proteins with capsids during egress (30, 51).

As studies on pathogens such as *Listeria monocytogenes* have propelled the understanding of actin polymerization and its regulation, we expect that determining the mechanism of directional transport of herpesvirus capsids will gain insight into the general underlining cell biology of coordinated bidirectional transport. In addition, regulation of capsid targeting in the peripheral nervous system may play an important role

in determining the outcome of viral infection and provide insights into the mechanism of herpesvirus encephalitis.

We thank K. Collier and S. Noles for their help with constructing viruses PRV-GS847 and PRV-GS791, respectively, and J. Goodhouse for his expert help with confocal microscopy. Members of the Enquist labora-

tory provided useful comments and discussion. G.A.S. was supported by a Scheppe Foundation award and, in part, by National Institutes of Health (NIH) Grant 1RO1AI056346. L.P. was supported by NIH Grant 1F32 NS04 2967-01A1. S.P.G. was supported in part by NIH Grant 1RO1GM64624. L.W.E. was supported by NIH National Institute of Neurological Disorders and Stroke Grant 1RO133506.

1. Enquist, L. W., Husak, P. J., Banfield, B. W. & Smith, G. A. (1998) *Adv. Virus Res.* **51**, 237–347.
2. Roizman, B. & Sears, E. (1996) in *Fundamental Virology*, eds. Fields, B. N., Knipe, D. M. & Howley, P. M. (Lippincott-Raven, Philadelphia), pp. 1043–1107.
3. Hinson, V. K. & Tyor, W. R. (2001) *Curr. Opin. Neurol.* **14**, 369–374.
4. Tomishima, M. J., Smith, G. A. & Enquist, L. W. (2001) *Traffic* **2**, 429–436.
5. Smith, G. A., Gross, S. P. & Enquist, L. W. (2001) *Proc. Natl. Acad. Sci. USA* **98**, 3466–3470.
6. Rietdorf, J., Ploubidou, A., Reckmann, I., Holmstrom, A., Frischknecht, F., Zetl, M., Zimmermann, T. & Way, M. (2001) *Nat. Cell Biol.* **3**, 992–1000.
7. Ward, B. M. & Moss, B. (2001) *J. Virol.* **75**, 4802–4813.
8. Campbell, R. E., Tour, O., Palmer, A. E., Steinbach, P. A., Baird, G. S., Zacharias, D. A. & Tsien, R. Y. (2002) *Proc. Natl. Acad. Sci. USA* **99**, 7877–7882.
9. Smith, G. A. & Enquist, L. W. (2000) *Proc. Natl. Acad. Sci. USA* **97**, 4873–4878.
10. Lee, E. C., Yu, D., Martinez de Velasco, J., Tessarollo, L., Swing, D. A., Court, D. L., Jenkins, N. A. & Copeland, N. G. (2001) *Genomics* **73**, 56–65.
11. Johnson, R. M. & Spear, P. G. (1989) *J. Virol.* **63**, 819–827.
12. Campadelli-Fiume, G., Arsenakis, M., Farabegoli, F. & Roizman, B. (1988) *J. Virol.* **62**, 159–167.
13. Peeters, B., de Wind, N., Hooisma, M., Wagenaar, F., Gielkens, A. & Moormann, R. (1992) *J. Virol.* **66**, 894–905.
14. Hollenbeck, P. J. (1993) *J. Cell Biol.* **121**, 305–315.
15. Lycke, E., Hamark, B., Johansson, M., Krotochwil, A., Lycke, J. & Svennerholm, B. (1988) *Arch. Virol.* **101**, 87–104.
16. Nicola, A. V., McEvoy, A. M. & Straus, S. E. (2003) *J. Virol.* **77**, 5324–5332.
17. Lycke, E., Kristensson, K., Svennerholm, B., Vahlne, A. & Ziegler, R. (1984) *J. Gen. Virol.* **65**, 55–64.
18. Banfield, B. W., Kaufman, J. D., Randall, J. A. & Pickard, G. E. (2003) *J. Virol.* **77**, 10106–10112.
19. Smeraski, C. A., Sollars, P. J., Ogilvie, M. D., Enquist, L. W. & Pickard, G. E. (2004) *J. Comp. Neurol.* **471**, 298–313.
20. Hollenbeck, P. J. & Bray, D. (1987) *J. Cell Biol.* **105**, 2827–2835.
21. Ahmari, S. E., Buchanan, J. & Smith, S. J. (2000) *Nat. Neurosci.* **3**, 445–451.
22. Kaether, C., Skehel, P. & Dotti, C. G. (2000) *Mol. Biol. Cell* **11**, 1213–1224.
23. Nakata, T., Terada, S. & Hirokawa, N. (1998) *J. Cell Biol.* **140**, 659–674.
24. Overly, C. C. & Hollenbeck, P. J. (1996) *J. Neurosci.* **16**, 6056–6064.
25. Mueller, S., Cao, X., Welker, R. & Wimmer, E. (2002) *J. Biol. Chem.* **277**, 7897–7904.
26. Marchand, C. F. & Schwab, M. E. (1986) *Brain Res.* **383**, 262–270.
27. Card, J. P., Rinaman, L., Lynn, R. B., Lee, B. H., Meade, R. P., Miselis, R. R. & Enquist, L. W. (1993) *J. Neurosci.* **13**, 2515–2539.
28. Penfold, M. E. T., Armati, P. & Cunningham, A. L. (1994) *Proc. Natl. Acad. Sci. USA* **91**, 6529–6533.
29. Miranda-Saksena, M., Armati, P., Boadle, R. A., Holland, D. J. & Cunningham, A. L. (2000) *J. Virol.* **74**, 1827–1839.
30. Holland, D. J., Miranda-Saksena, M., Boadle, R. A., Armati, P. & Cunningham, A. L. (1999) *J. Virol.* **73**, 8503–8511.
31. Tomishima, M. J. & Enquist, L. W. (2001) *J. Cell Biol.* **154**, 741–752.
32. Deacon, S. W., Serpinskaya, A. S., Vaughan, P. S., Lopez Fanarraga, M., Vernos, I., Vaughan, K. T. & Gelfand, V. I. (2003) *J. Cell Biol.* **160**, 297–301.
33. Ligon, L. A., Tokito, M., Finkelstein, J. M., Grossman, F. E. & Holzbaur, E. L. (2004) *J. Biol. Chem.* **279**, 19201–19208.
34. Martinez-Moreno, M., Navarro-Lerida, I., Roncal, F., Albar, J. P., Alonso, C., Gavilanes, F. & Rodriguez-Crespo, I. (2003) *FEBS Lett.* **544**, 262–267.
35. Douglas, M. W., Diefenbach, R. J., Homa, F. L., Miranda-Saksena, M., Rixon, F. J., Vittone, V., Byth, K. & Cunningham, A. L. (2004) *J. Biol. Chem.* **279**, 28522–28530.
36. Diefenbach, R. J., Miranda-Saksena, M., Diefenbach, E., Holland, D. J., Boadle, R. A., Armati, P. J. & Cunningham, A. L. (2002) *J. Virol.* **76**, 3282–3291.
37. Ye, G. J., Vaughan, K. T., Vallee, R. B. & Roizman, B. (2000) *J. Virol.* **74**, 1355–1363.
38. Dohner, K., Wolfstein, A., Prank, U., Echeverri, C., Dujardin, D., Vallee, R. & Sodeik, B. (2002) *Mol. Biol. Cell* **13**, 2795–2809.
39. Sodeik, B., Ebersold, M. W. & Helenius, A. (1997) *J. Cell Biol.* **136**, 1007–1021.
40. Welte, M. A., Gross, S. P., Postner, M., Block, S. M. & Wieschaus, E. F. (1998) *Cell* **92**, 547–557.
41. Gross, S. P., Tuma, M. C., Deacon, S. W., Serpinskaya, A. S., Reilein, A. R. & Gelfand, V. I. (2002) *J. Cell Biol.* **156**, 855–865.
42. Chada, S. R. & Hollenbeck, P. J. (2003) *J. Exp. Biol.* **206**, 1985–1992.
43. Gross, S. P., Welte, M. A., Block, S. M. & Wieschaus, E. F. (2002) *J. Cell Biol.* **156**, 715–724.
44. Rodionov, V., Yi, J., Kashina, A., Oladipo, A. & Gross, S. P. (2003) *Curr. Biol.* **13**, 1837–1847.
45. Gross, S. P., Guo, Y., Martinez, J. E. & Welte, M. A. (2003) *Curr. Biol.* **13**, 1660–1668.
46. Zhang, G., Stevens, R. & Leader, D. P. (1990) *J. Gen. Virol.* **71**, 1757–1765.
47. Coulter, L. J., Moss, H. W., Lang, J. & McGeoch, D. J. (1993) *J. Gen. Virol.* **74**, 387–395.
48. Overton, H. A., McMillan, D. J., Klavinskis, L. S., Hope, L., Ritchie, A. J. & Wong-kai-in, P. (1992) *Virology* **190**, 184–192.
49. Cunningham, C., Davison, A. J., Dolan, A., Frame, M. C., McGeoch, D. J., Meredith, D. M., Moss, H. W. & Orr, A. C. (1992) *J. Gen. Virol.* **73**, 303–311.
50. Muresan, V., Godek, C. P., Reese, T. S. & Schnapp, B. J. (1996) *J. Cell Biol.* **135**, 383–397.
51. Miranda-Saksena, M., Boadle, R. A., Armati, P. & Cunningham, A. L. (2002) *J. Virol.* **76**, 9934–9951.